

# SKYRME-RPA DESCRIPTION OF DIPOLE GIANT RESONANCE IN HEAVY AND SUPERHEAVY NUCLEI

W. Kleinig<sup>1,2</sup>, V.O. Nesterenko<sup>1</sup>, J. Kvasil<sup>3</sup>, P.-G. Reinhard<sup>4</sup> and P. Vesely<sup>3</sup>

<sup>1</sup> *Laboratory of Theoretical Physics, Joint Institute for Nuclear Research, Dubna, Moscow region, 141980, Russia\**

<sup>2</sup> *Technische Universität Dresden, Inst. für Analysis, D-01062, Dresden, Germany*

<sup>3</sup> *Institute of Particle and Nuclear Physics, Charles University, CZ-18000, Praha 8, Czech Republic and*

<sup>4</sup> *Institut für Theoretische Physik II, Universität Erlangen, D-91058, Erlangen, Germany*

(Dated: November 1, 2018)

The E1(T=1) isovector dipole giant resonance (GDR) in heavy and super-heavy deformed nuclei is analyzed over a sample of 18 rare-earth nuclei, 4 actinides and three chains of super-heavy elements (Z=102, 114 and 120). Basis of the description is self-consistent separable RPA (SRPA) using the Skyrme force SLy6. The self-consistent model well reproduces the experimental data (energies and widths) in the rare-earth and actinide region. The trend of the resonance peak energies follows the estimates from collective models, showing a bias to the volume mode for the rare-earths isotopes and a mix of volume and surface modes for actinides and super-heavy elements. The widths of the GDR are mainly determined by the Landau fragmentation which in turn is found to be strongly influenced by deformation. A deformation splitting of the GDR can contribute about one third to the width and about 1 MeV further broadening can be associated to mechanism beyond the mean-field description (escape, coupling with complex configurations).

## I. INTRODUCTION

The isovector giant dipole resonance (GDR) is a most prominent and much studied excitation mode of nuclei, see e.g. [1, 2]. Nonetheless, it remains a subject of actual interest as there are many aspects which deserve more detailed investigations as, e.g., photo-excitation cross sections in exotic nuclei which play a role in astrophysical reaction chains [3] or isotopic trends of the GDR including the regimes of deformed nuclei. The present paper aims at a theoretical survey of the GDR in isotopic chains of heavy and super-heavy nuclei.

The high importance of the GDR has triggered since long many theoretical surveys analyzing the intriguing aspects of nuclear collective motion, starting from a purely collective description [4, 5] and slowly establishing a link to microscopic models in the framework of the Random-Phase Approximation (RPA) [6, 7]. The theoretical description has much developed over the years. The majority of RPA investigations in the past employed shell model potentials plus an effective residual interaction (Migdal theory) [8, 9, 10]. In the meantime, self-consistent nuclear models have been steadily improving towards a reliable description of nuclear structure and excitations, for reviews see, e.g., [11, 12, 13]. These models belong to the class of density functional methods which aim at a universal energy functional for a given system from which all static and dynamics equations are derived in a strictly variational frame [14, 15]. Such density functional models, being rather universal by construction, are promising for investigation in exotic areas, e.g. for r-process, drip-line and super-heavy nuclei. The studies in this paper are based on the Skyrme functional which has

been introduced in [16, 17] and extended to a dynamical description shortly after [18, 19, 20]. The performance of self-consistent RPA calculations using the Skyrme functional had been tested systematically in [21, 22] and it was found that one can have a reliable description when taking care to chose an appropriate parametrization.

Systematic scans through the isotopic landscape and the study of exotic nuclei run over many deformed nuclei. Fully fledged RPA calculations for deformed nuclei are feasible [23], but extremely time consuming, not suited for systematic investigations. Super-heavy nuclei are especially demanding due to a coexistence of two obstacles, large size and deformation. Accurate but less demanding RPA techniques are needed. To that end, the separable RPA (SRPA) based on the Skyrme functional was recently developed [24, 25]. The self-consistent factorization of the residual interaction in SRPA reduces the computational expense dramatically and so gives way to systematic explorations of nuclear giant resonances in both spherical and deformed nuclei [24]-[28]. In this paper we concentrate on the isovector (T=1) electric GDR.

As was shown in our previous studies [24]-[28], SRPA provides an accurate description of the GDR in spherical and deformed nuclei. We obtained good agreement with experiment for <sup>154</sup>Sm, <sup>238</sup>U and Nd isotopes with A=142, 144, 146, 148, 150. Eight different Skyrme forces were checked in these investigations. In this paper, we aim at a large systematics over the isotopic landscape and decide for one parameterization, namely SLy6 [29] which was found to provide a satisfying description of the GDR for spherical and deformed nuclei. In a first step, SRPA results for the GDR will be compared with all available experiment data in rare-earth and actinide regions. In particular, we consider nuclei <sup>156,160</sup>Gd, <sup>166,168</sup>Er, <sup>170,172,174,176</sup>Yb, <sup>176,178,180</sup>Hf, <sup>182,184,186</sup>W, <sup>186,188,190,192</sup>Os, <sup>232</sup>Th and <sup>234,236,238</sup>U. Basic characteristics (energy centroid, width, deformation

\*Electronic address: nester@theor.jinr.ru

splitting) and their trends with system size will be analyzed.

In a second step, we will investigate the GDR in super-heavy nuclei for the three isotopic chains: Nobelium with  $Z=102$  ( $A=242, 248, 254, 262, 270$ ),  $Z=114$  ( $A=264, 274, 284, 294, 304$ ) and  $Z=120$  ( $A=280, 288, 294, 304, 312$ ). As discussed below, this set covers most of the important mass regions and so is sufficiently representative. The main features of the GDR are analyzed and compared with those in rare-earth and actinide region.

The paper is organized as follows. The calculation scheme, methods of analysis and choice of the isotopes are sketched in Sec. II. In Sec. III the results of the calculations for the GDR in rare-earth, actinide and super-heavy nuclei are discussed. A summary is done in Sec. IV.

## II. FRAMEWORK

The calculations are performed in the framework of SRPA [28] with the Skyrme force SLy6 [29] which provides a satisfying description of the GDR for heavy nuclei [25, 26, 27, 28]. The contribution to the residual interaction from the time-odd current density, Coulomb and pairing (at the BCS level) are taken into account [25]. The calculations employ a cylindrical coordinate-space grid with the mesh size 0.7 fm. The calculation box has 24-35 mesh points depending on the nuclear size and deformation. For generators of the separable interaction, we use four input operators,  $rY_{1\mu}$  and  $j(q_i r)Y_{1\mu}$ ,  $i = 1, 2, 3$ , with  $q_i$  chosen following the prescription [24]. These operators are shown to give accurate results in spherical nuclei [24]. Besides, the operator  $r^3 Y_{3\mu}$  is added to take into account the multipole mixing of excitations with the same projection  $\mu$  and space parity  $\pi$ .

For all nuclei, the equilibrium quadrupole deformations are found by minimization of the total energy. The deformations are characterized by the charge quadrupole moments  $Q_2$  and related dimensionless parameters  $\beta_2$  as

$$Q_2 = \int d\vec{r} \rho_p(\vec{r}) r^2 Y_{20}, \quad \beta_2 = \sqrt{\frac{\pi}{5}} \frac{Q_2}{Z \langle r^2 \rangle_p} \quad (1)$$

where  $\rho_p(\vec{r})$  is the proton density in the ground state,  $\langle r^2 \rangle_p = \int d\vec{r} \rho_p(\vec{r}) r^2 / Z$  is the r.m.s. proton radius and  $Z$  is the number of protons.

The calculations use a large basis space of single-particle states to expand the SRPA operators with two-quasiparticle states extending up to  $\sim 65$  MeV, see Table I. The energy-weighted sum rule

$$EWSR(T=1, \lambda=1) = 9 \frac{(\hbar c)^2}{8\pi m_1^*} \frac{NZ}{A} \quad (2)$$

is then exhausted by 92-95%. This sum rule includes the isovector effective mass  $m_1^*$  as the velocity-dependent terms are involved to the calculations, see discussion in [28]. In SLy6 we have actually  $m_1^*/m=0.80$ .

TABLE I: Characteristics of the configuration space used in the calculations: minimal  $E_{min}$  and maximal  $E_{max}$  single-particle energies, number of the single-particle levels  $K$  for protons and neutrons, number of two-quasiparticle dipole states  $N_{2qp}$  (for branches  $\mu = 0$  and 1 altogether). See text for more details.

Nucleus	$E_{min}, E_{max}$		K		$N_{2qp}$
	Z	N	Z	N	
<sup>154</sup> Gd	-45.4, +20.2	-57.2, +17.0	252	308	4720
<sup>238</sup> U	-42.7, +19.3	-58.0, +14.8	307	393	6860
<sup>294</sup> 120	-36.4, +20.9	-58.7, +14.1	360	426	8720

Since SRPA includes the dipole time-odd momentum-like operators [25], the center-of-mass mode should, in principle, be placed correctly at zero energy. However, the finite computational box breaks translational invariance such that the spurious isoscalar E1 strength becomes concentrated at the region of 2-3 MeV. That is safely below the GDR which we are studying here.

The energy-weighted isovector dipole strength function is computed as

$$S(E1\mu; \omega) = \sum_{\nu} \omega_{\nu} \langle \Psi_{\nu} | \hat{E}_{1\mu} | \Psi_0 \rangle \zeta(\omega - \omega_{\nu}) \quad , \quad (3)$$

$$\hat{E}_{1\mu} = \frac{N}{A} \sum_{p=1}^Z r_p Y_{1\mu}(\Omega_p) - \frac{Z}{A} \sum_{n=1}^N r_n Y_{1\mu}(\Omega_n) \quad ,$$

smoothed by the Lorentz function

$$\zeta(\omega - \omega_{\nu}) = \frac{1}{2\pi} \frac{\Delta}{(\omega - \omega_{\nu})^2 + \frac{\Delta^2}{4}} \quad (4)$$

with the averaging parameter  $\Delta=2$  MeV in most of the calculations. That averaging width was found to be optimal for the comparison with experiment and simulation of broadening effects beyond SRPA (escape widths, coupling with complex configurations). Further,  $\Psi_0$  is the ground state,  $\nu$  runs over the RPA spectrum with eigenfrequency  $\omega_{\nu}$  and eigenstate  $|\Psi_{\nu}\rangle$ .

To estimate the resonance energy centroid  $E$ , width  $\Gamma$ , and deformation splitting  $\Delta E$ , the following prescriptions are applied. To determine  $E$ , the energy interval around the resonance with the strength larger than 10% of the maximal value is used and the centroid of the strength inside this interval is determined. The same method is implemented to find centroids  $E_0$  and  $E_1$  of  $\mu = 0$  and 1 branches separately. Then the deformation splitting  $\Delta E = E_1 - E_0$  is obtained. The width  $\Gamma$  is determined at a half-maximum of the resonance.

The experimental data for the GDR [30, 31, 32, 33, 34, 35, 36, 37, 38, 39] include photoabsorption

$$\sigma = (\gamma, n) + (\gamma, p) + (\gamma, np) + (\gamma, 2n) + (\gamma, d) + \dots + (\gamma, f) \quad ,$$

neutron yield

$$\sigma = (\gamma, n) + (\gamma, np) + 2(\gamma, 2n) + 3(\gamma, 3n) + \dots + (\gamma, f) \quad ,$$

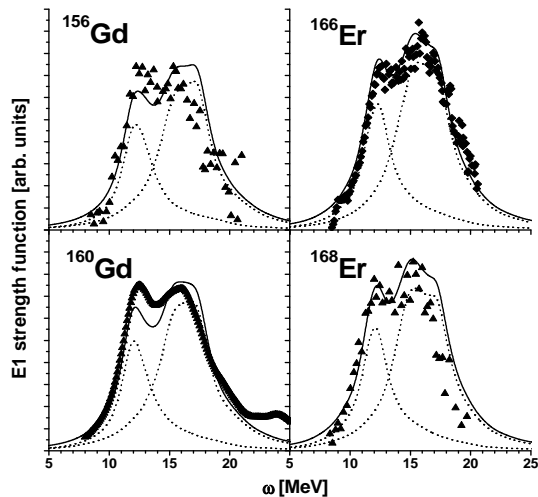


FIG. 1: Isovector dipole strength in  $^{156,160}\text{Gd}$  and  $^{166,168}\text{Er}$ . The calculated strength (solid curve) is compared with the experimental data for total photoabsorption [31, 32] (triangles) and neutron product [33] (rhombus). The branches of the resonance with  $\mu = 0$  (left small) and  $\mu = 1$  (right large) are represented by dotted curves. The deformations are  $\beta_2=0.347$ , 0.359 and 0.348, 0.353, respectively.

and neutron product

$$\sigma = (\gamma, n) + (\gamma, np) + (\gamma, 2n) + (\gamma, 3n) + \dots + (\gamma, f) .$$

The photoabsorption data are preferable as involving all the main decay channels and so most corresponding to the strength function (3). If the photoabsorption data are absent, the neutron yield and neutron product can be also used for a rough comparison since these data include most of the main channels. However, one should take into account that both neutron yield and product omit  $(\gamma, p)$  channel and so can underestimate the strength and change the resonance gross-structure. Besides, the neutron yield amplifies the neutron contributions  $(\gamma, 2n), (\gamma, 3n), \dots$  and hence the right wing of the resonance. In what follows, we use experimental data for photoabsorption in  $^{156}\text{Gd}$  [31],  $^{160}\text{Gd}$  [32],  $^{168}\text{Er}$  [31],  $^{174}\text{Yb}$  [31],  $^{178,180}\text{Hf}$  [31],  $^{182,184,186}\text{W}$  [31],  $^{232}\text{Th}$  [37],  $^{238}\text{U}$  [37], neutron yield in  $^{170,172,176}\text{Yb}$  [34],  $^{186,188,190,192}\text{Os}$  [36], neutron products  $(\gamma, n) + (\gamma, np) + (\gamma, 2n)$  in  $^{166}\text{Er}$  [33],  $^{176}\text{Hf}$  [35] and  $(\gamma, n) + (\gamma, np) + (\gamma, 2n) + (\gamma, f)$  in  $^{234}\text{U}$  [38],  $^{236}\text{U}$  [39].

In rare-earth and actinide regions, we consider all nuclei for which reasonable GDR experimental data exist (for exception of Nd and Sm isotopes already explored in our previous papers [25, 26, 27, 28]). In super-heavy nuclei, we look at three isotopic chains: Nobelium  $Z=102$  ( $A=242, 248, 254, 262, 270$ ),  $Z=114$  ( $A=264, 274, 284, 294, 304$ ) and  $Z=120$  ( $A=280, 288, 294, 304, 312$ ). As can be seen from [46], these chains cover most interesting mass and deformation regions. Indeed, they involve the onset ( $Z=102$ ), the center ( $Z=114$ ) and the upper end ( $Z=120$ ) of the super-heavy region. Every chain extends through the whole neutron interval at a given  $Z$ .

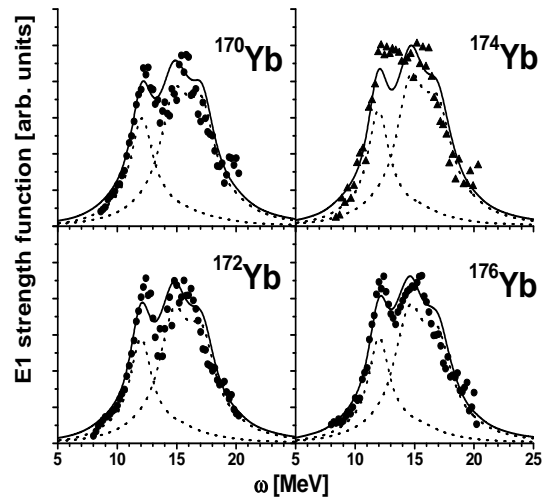


FIG. 2: Same as in Fig. 1 for  $^{170,172,174,176}\text{Yb}$ . The experimental data are for neutron yield [34] (closed circles) and total photoabsorption [31] (triangles). The deformation parameters are  $\beta_2=0.350, 0.347, 0.340, 0.327$ , respectively.

Different deformation regions are covered. For  $Z=102$  we deal with well deformed nuclei and small variation of the quadrupole deformation. The chains  $Z=114$  and  $120$  show strong variations of the deformation with a strong decrease with increasing  $N$ , i.e. when moving towards the magic neutron number  $N=184$  [40]. The proton numbers  $Z=114$  and  $120$  are tentatively magic [11, 41] such that neutron shell structure acquires a decisive weight for sphericity or deformation.

### III. RESULTS AND DISCUSSION

#### A. Rare-earth and actinide nuclei

Results of SRPA calculations for rare-earth and actinide nuclei are presented in Figs. 1-6. Note that for reasons of comparison the calculated strength function is rescaled so as to correspond roughly to the maximal magnitude of the experimental cross section. Moreover, because of the insufficient accuracy of the model and experimental resolution (see discussion in the previous section) we skip here the analysis of the fine structure which manifests itself mainly at the top of the resonance. The main attention will be paid the resonance energy centroids and widths.

Figures 1 and 2 show an excellent agreement with experiment for Gd, Er and Yb isotopes. The agreement is less perfect for Hf, W and Os shown in Figures 3 and 4: the calculated strength exhibits a slight ( $\sim 0.5$  MeV) down-shift in Hf and W and a larger ( $\sim 1$  MeV) up-shift in Os. It is known that Os isotopes are soft to oblate quadrupole deformation, which is confirmed by our calculations. However, as we checked, SRPA calculations on

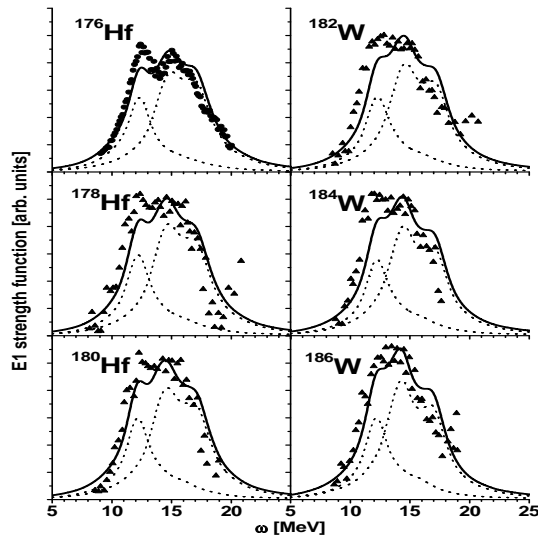


FIG. 3: Same as in Fig. 1 for  $^{176,178,180}\text{Hf}$  and  $^{182,184,186}\text{W}$ . The experimental data are for total photoabsorption [31] (triangles) and neutron product [35] (closed circles). The deformation parameters for  $^{176,178,180}\text{Hf}$  and  $^{182,184,186}\text{W}$  are  $\beta_2=0.330, 0.296, 0.287$  and  $0.260, 0.252, 0.247$ , respectively.

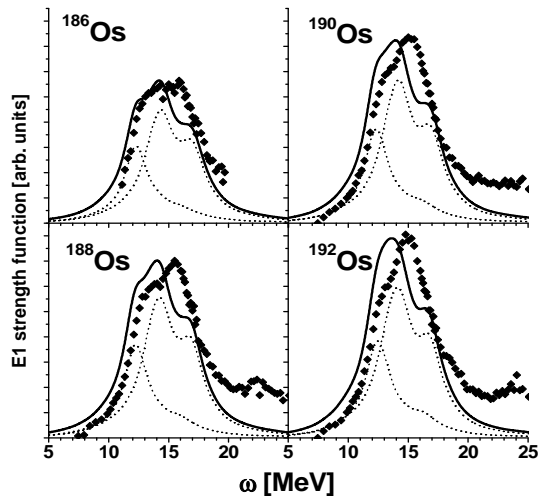


FIG. 4: Same as in Fig. 1 for  $^{186,188,190,192}\text{Os}$ . The experimental data are for neutron yield [36] (rhombus). The deformation parameters are  $\beta_2=0.222, 0.217, 0.195, 0.172$ , respectively.

top of the oblate isomer do not improve agreement with the experiment. The discrepancies for Os may be partly caused by using the neutron yield experimental data. As was discussed above, the neutron yield alone can amplify the right GDR flank, thus resulting in some apparent up-shift as compared with the total photoabsorption cross section. Results for the actinides in Fig. 5 also look encouraging. Modest deviations in gross-structure of  $^{234,236}\text{U}$  can be explained by using the neutron product experimental data.

It is worth noting that the comprehensive analysis of

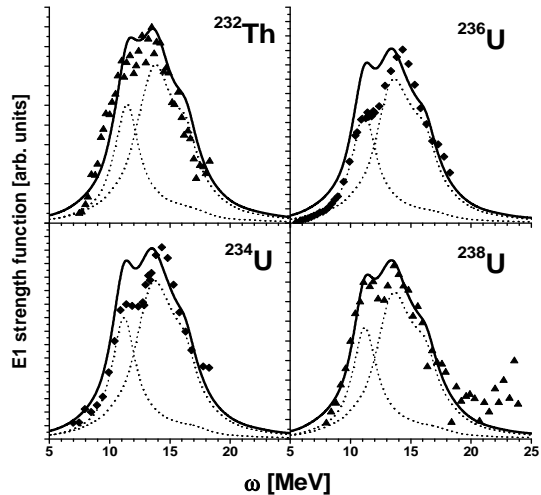


FIG. 5: Same as in Fig. 1 for  $^{232}\text{Th}$  and  $^{234,236,238}\text{U}$ . The experimental data are for total photoabsorption [37] (triangles) and neutron product [38, 39] (rhombus). The deformation parameters for  $^{232}\text{Th}$  and  $^{234,236,238}\text{U}$  are  $\beta_2=0.256$  and  $0.279, 0.286, 0.287$ , respectively.

experimental data reveals noticeable (sometimes significant) deviations in GDR measurements of different experimental groups [42]. Taking into account these uncertainties in the data, one may consider for all cases above the agreement with experimental data as very satisfying, at least for energy centroids and widths.

The correlation of the quadrupole moments (1) with some resonance characteristics (width  $\Gamma$ , deformation splitting  $\Delta E$ , energy centroid  $E$ ) and trends of these characteristics with the mass number  $A$  are shown in Fig. 6. All nuclei in the sample have a significant quadrupole deformation. The calculated quadrupole moments are in excellent agreement with the experiment [43]. In the rare-earth nuclei the moments have a maximum in the middle of the region. Note that the dimensionless deformation parameters  $\beta_2$  as indicated in the captions of the previous figures are maximal at the onset of the region. The difference between  $Q_2$  and  $\beta_2$  maxima is related with the nuclear mass factor in (1). The direct contribution of the deformation splitting  $\Delta E$  to the resonance width is maximal ( $\sim 40\%$ ) in the first half of the region ( $A < 176$ ) and then slowly decreases to 37 – 34% for Hf, 34 – 31% for W and 31 – 24% for Os. Furthermore,  $\Delta E$  is a bit increased in actinides where it reaches 30 – 33%. This trend obviously correlates with  $\beta_2$ . See also the detailed discussion of the GDR width and structure in section III C.

In Figure 6c, the resonance energy is compared with empirical estimates based on Steinwedel-Jensen (SJ) [5]

$$E_{SJ} = 81A^{-1/3}\text{MeV} \quad (5)$$

and Berman-Fultz (BF) [1, 2]

$$E_{BF} = (31.2A^{-1/3} + 20.6A^{-1/6})\text{MeV} \quad (6)$$

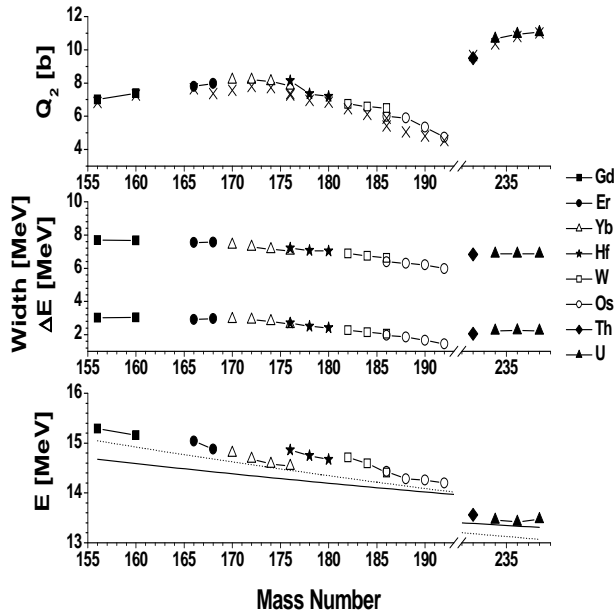


FIG. 6: Calculated characteristics of rare-earth and actinide nuclei as function of mass number. Upper panel: Quadrupole moments  $Q_2$  compared with experimental values (crosses) [43]. Middle panel: Widths  $\Gamma$  (upper set) and deformation splittings  $\Delta E$  (lower set). Lower panel: Energy centroids as compared with the estimates (5) (dotted curve) and (6) (solid curve).

collective models. BF takes into account both volume and surface contributions and treats the dipole resonance as a combination of Steinwedel-Jensen [5] and Goldhaber-Teller (GT) [4] scenarios. The calculated energies are closer to the SJ estimate (5) in the rare-earth region and to the BF estimate (6) in actinides. As shown below, the BF estimate is also more appropriate in super-heavy nuclei. This agrees with a commonly accepted view that in heavy nuclei neither the density gradient ( $\sim A^{-1/3}$ ) nor the nuclear surface impact ( $\sim A^{-1/6}$ ) dominate the restoring force [2, 44, 45].

### B. Super-heavy nuclei

The agreement of SRPA results with the experimental data in rare-earth and actinide nuclei encourages its further application to super-heavy nuclei. SRPA results for super-heavy nuclei are exhibited in Figs. 7-10.

Fig. 7 indicates that the GDR in this region is generally similar to that in rare-earth and actinide nuclei. In particular, the resonance width correlates with the quadrupole parameter  $\beta_2$ . Furthermore, the middle panels in Figs. 8-10 show that the direct contribution of the deformation splitting  $\Delta E$  to the resonance width  $\Gamma$  does not exceed 40%, as in rare-earth and actinide nuclei. Note that our quadrupole moments  $Q_2$  from the

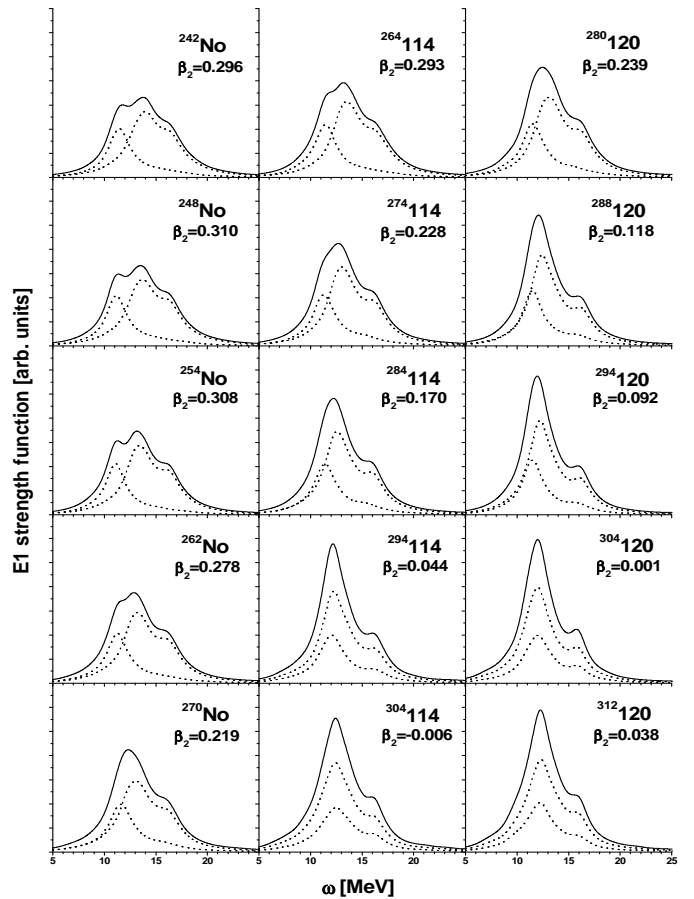


FIG. 7: Same as in Fig. 1 for isotopes of super-heavy nuclei No and  $Z=114$  and  $120$ . The dimensionless proton quadrupole deformation  $\beta_2$  is indicated in the plots.

self-consistent calculations agree nicely with the values obtained within the macroscopic-microscopic model [46], see the upper panels in Figs. 8-10. The agreement persists even in mass regions with large variations of deformation.

At the same time, the GDR in super-heavy nuclei shows some peculiarities. First, unlike the rare-earth nuclei, its energy is much closer to the BF estimate (6) than to (5), which supports once again the treatment of the GDR in heavy nuclei as a mixture of SJ and GT modes. Maximal deviations from both estimates emerge at the ends of the isotopic chains, which is natural since these estimates do not parameterize any isospin dependence. Second, as is seen from Figs. 8-10, the decrease of the resonance energies with neutron number  $N$  levels off and is even reversed to some increase at the end of every isotope chain. This can be explained by increase of the symmetry energy  $E \propto E_{sym} = a_{sym}(N - Z)^2/A^2$  at these neutron-rich edges. Note that such a turnover is absent for lighter nuclei, e.g. in the chain of Nd isotopes ( $A=134-158$ ) explored earlier in [28]. Probably this is because Nd isotopes do not reach so large neutron excess as the super-heavy elements.

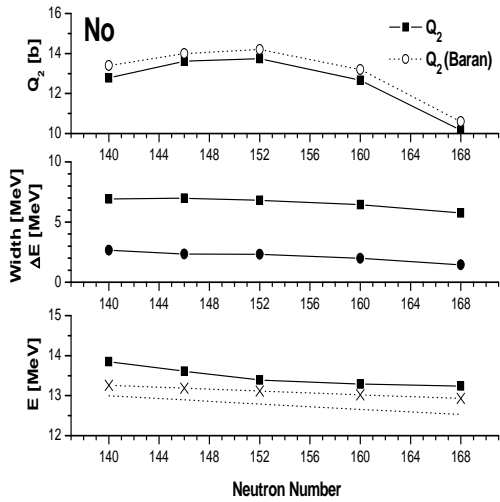


FIG. 8: Calculated characteristics of No isotopes as a function of their neutron number. Upper panel: Quadrupole moments  $Q_2$  (black squares) as compared with the values [46] (open circles). Middle panel: Widths  $\Gamma$  (black squares) and deformation splittings  $\Delta E$  (black circles). Lower panel: Energy centroids (black squares) as compared with the estimates  $E_{SJ}$  (5) (dotted curve) and  $E_{BF}$  (6) (dotted curve with crosses).

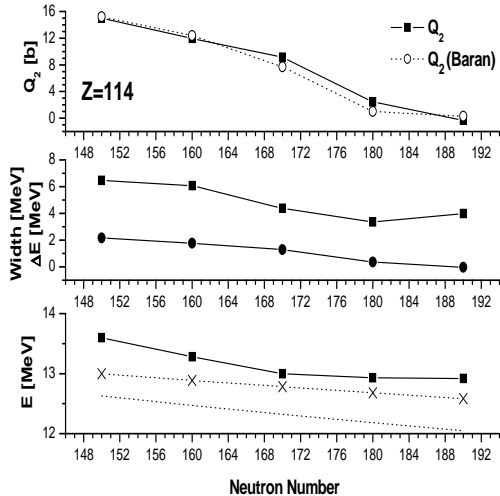


FIG. 9: Same as in Fig. 8 for  $Z=114$  isotopes.

### C. GDR width and structure: general discussion

In Figure 11, the isovector dipole strengths calculated with different Lorentz averaging parameter  $\Delta$  are compared for a representative set of nuclei. It is seen that smaller averaging,  $\Delta = 0.5$  and 1 MeV, yields more fine structures, mainly at the resonance peak, and leaves the total width almost unchanged. As a rule,  $\delta\Gamma = \Gamma(\Delta = 2 \text{ MeV}) - \Gamma(\Delta = 0.5 \text{ MeV}) \leq 1 \text{ MeV}$ . Since  $\Gamma(\Delta = 2 \text{ MeV})$  well reproduces the experimental widths, one may associate the difference  $\delta\Gamma$  to the smoothing effects omitted in the present RPA calculations (coupling with complex configurations, escape widths). In fact, the averaging

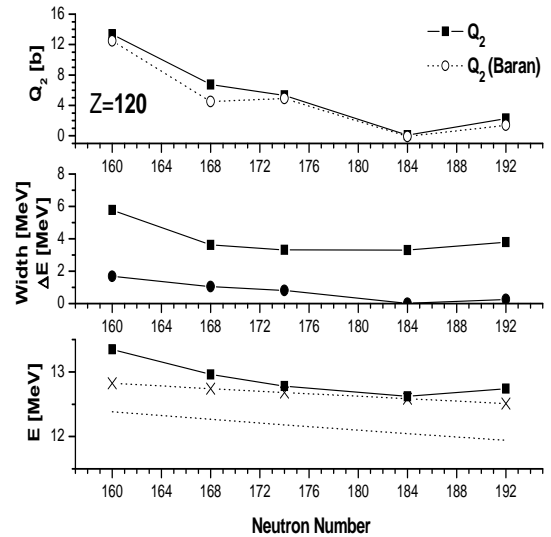


FIG. 10: Same as in Fig. 8 for  $Z=120$  isotopes.

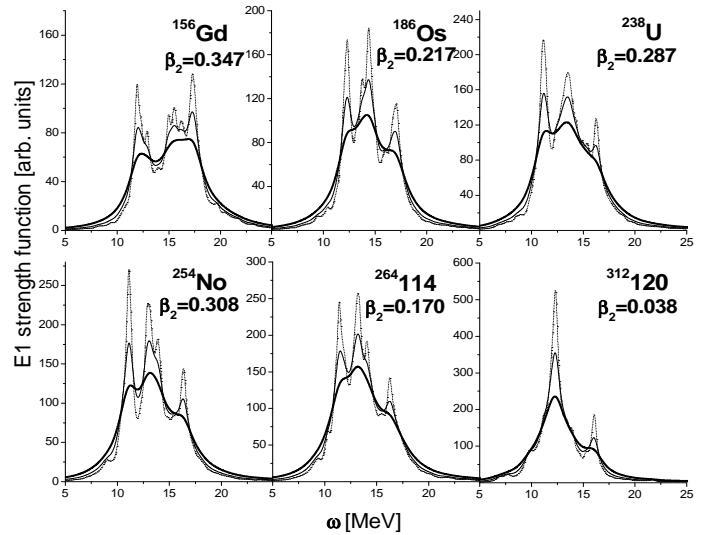


FIG. 11: The isovector dipole strength calculated with different averaging in the strength function (3):  $\Delta = 0.5$  MeV (dash curve), 1 MeV (thin solid curve), and 2 MeV (bold solid curve). The parameters of the proton quadrupole deformation are given for every nucleus.

with  $\Delta = 2$  MeV effectively mimics these effects. Since  $\delta\Gamma \ll \Gamma(\Delta = 2 \text{ MeV})$ , the deformation splitting and Landau fragmentation (distribution of the collective strength between nearby two-quasiparticle states) obviously dominate the total width. We estimate their contribution by 70-90%, depending on the nucleus and its shape.

Figure 11 also shows that the averaging  $\Delta = 2$  MeV chosen in our calculations is indeed most suitable for the comparison with the GDR experimental data (at least for the heavy nuclei considered here). This averaging does not cause significant artificial increase of the resonance width and, at the same time, allows to suppress the structure details which, in any case, are not resolved

TABLE II: Calculated RPA widths  $\Gamma_0$  and  $\Gamma_1$  of the resonance branches  $\mu = 0$  and 1, the sum  $\Gamma_0 + \Gamma_1$ , and the total width  $\Gamma$ . For every nucleus the deformation parameters  $\beta_2$  are given. The averaging is  $\Delta = 2\text{MeV}$ . For more details see the text.

Nucleus	$\beta_2$	Widths [MeV]			
		$\Gamma_0$	$\Gamma_1$	$\Gamma_0 + \Gamma_1$	$\Gamma$
$^{156}\text{Gd}$	0.347	3,05	4,74	7,79	7,69
$^{172}\text{Yb}$	0.347	2,54	5,08	7,62	7,28
$^{186}\text{Os}$	0.222	2,65	5,09	7,74	6,39
$^{238}\text{U}$	0.287	2,62	5,11	7,73	6,86
$^{254}\text{No}$	0.308	2,44	5,13	7,57	6,81
$^{264}_{114}$	0.293	2,74	5,11	7,85	6,47
$^{304}_{114}$	-0.006	3,98	3,99	7,97	3,98
$^{304}_{120}$	0.001	3,32	3,26	6,58	3,30
$^{312}_{120}$	0.038	3,61	3,91	7,52	3,80

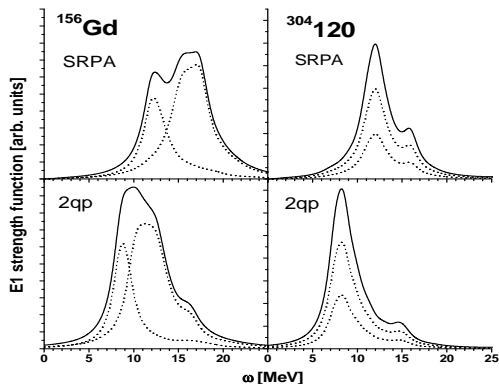


FIG. 12: The isovector dipole strength calculated with smoothing  $\Delta = 2\text{ MeV}$  in deformed  $^{156}\text{Gd}$  and spherical  $^{304}_{120}$ . The upper panels show full SRPA results (with residual interaction) and the lower panels pure two-quasiparticle (2qp) strengths (without residual interaction). The separate branches  $\mu=0$  (small) and  $\mu=1$  (large) are plotted by the dotted line and their sum by the full line.

in the experimental strength distributions.

Besides the splitting of the GDR into two branches, the deformation also results in a considerable redistribution of the strength within every branch. In other words, the deformation severely influences the Landau fragmentation itself. This effect is illustrated in Table II and Fig. 12. Table II provides the widths of the resonance branches  $\mu = 0$  and  $\mu = 1$  for a selection of nuclei. There is a large difference between spherical and deformed nuclei. In spherical nuclei ( $^{304}_{114}$ ,  $^{304}_{120}$ ,  $^{312}_{120}$ ), we have  $\Gamma_0 \approx \Gamma_1 \approx \Gamma$ , while in deformed nuclei,  $\Gamma_1 > \Gamma_0$  and their sum  $\Gamma_0 + \Gamma_1$  roughly covers the total width  $\Gamma$ . So, we see a strong deformation effect within the branches themselves. In order to analyze it, we plot in the lower panels of Fig. 12 the unperturbed two-quasiparticle (2qp) strengths. In deformed nuclei ( $^{156}\text{Gd}$ ) the inequality  $\Gamma_1 > \Gamma_0$  appears already in 2qp strengths, which shows that this is simply an effect of the density of states. The residual interac-

tion (SRPA case) does not cause essential changes in the relation between  $\mu = 0$  and  $\mu = 1$  branches and preserves  $\Gamma_1 > \Gamma_0$  in deformed nuclei. Besides showing the influence of deformation, Fig. 12 also illustrates the collective shifts from the unperturbed strengths to the final ones. The size of the shifts is, of course, related to the actual force SLy6. The shifts are 4.0 and 3.4 MeV in  $^{156}\text{Gd}$  and  $^{304}_{120}$ , respectively.

In most of the nuclei the calculations indicate a small shoulder at the right flank of the resonance. The heavier the nucleus, the stronger the shoulder. At a small averaging width, the shoulder becomes more pronounced and may even show up as a separate peak, see e.g. results for  $\Delta=0.5\text{ MeV}$  in Fig. 11. This effect is often absent, at least much less pronounced, in the experimental data. The shoulder takes place in both deformed and spherical nuclei and so is independent of deformation. It persists not only for SLy6 but also for most of other Skyrme forces [25, 26]. As was shown in [26], the effect is caused by specific 2qp structures with high angular momentum (thus large statistical weight) lying at the right GDR flank. It is to be noted that RPA neglects some broadening mechanisms (escape widths, coupling with complex, 2p-2h, etc, configurations) which could soften these structures. The shoulder can be further enhanced if the Skyrme force overestimates the dipole collective shift [25, 26]. The case calls for further detailed exploration.

#### IV. CONCLUSIONS

The isovector giant dipole resonance (GDR) is systematically investigated in rare-earth, actinide and super-heavy regions. The study covers 37 nuclei altogether. Mainly axially deformed nuclei are considered. In all the nuclei, the calculated quadrupole moments correctly reproduce the experimental data (rare-earth and actinide regions) [43] or macroscopic-microscopic estimates (super-heavy region) [46]. The calculations are performed in the framework of the self-consistent separable RPA approach (SRPA) based on the Skyrme functional. The force SLy6 is used.

A satisfying agreement of the SRPA results with the available GDR experimental data is found for 22 rare-earth and actinide nuclei. Resonance energies and widths are well described. The trends of the peak energies are compared with simple estimates from collective models. It is confirmed that the Steinwedel-Jensen (SJ) model performs well for medium heavy nuclei while a mix of SJ and the Goldhaber-Teller scenarios is more appropriate for heavy nuclei. Encouraged by these results, the survey is extended to super-heavy nuclei where GDR in isotope chains with  $Z=102$ , 114 and 120 are explored. The GDR in super-heavy nuclei is found to behave similar to that in rare-earth and actinide nuclei. The peak energies are, again, better described by the mixed collective model, continuing the trend from heavy nuclei. A new feature in the super-heavy region is that the peak energies turn

from decrease to increase towards the neutron rich ends of the isotopic chains (close to the drip lines).

We also analyze the GDR widths  $\Gamma$ . They are shown to be strictly dominated (at least 70-90%) by Landau fragmentation and deformation contributions. The direct deformation contribution through the splitting of the GDR into  $\mu = 0$  and 1 branches achieves 40%. The Landau fragmentation is severely affected by the deformation as well, which modifies the branch widths and lead to  $\Gamma_1 > \Gamma_0$ . The final step to agreement with experimental pattern is achieved by Lorentz averaging the SRPA results, thus simulating missing broadening mechanisms (e.g., escape widths and coupling with complex configurations). A modest additional broadening of  $\sim 1$  MeV suffices to reach realistic pattern.

## Acknowledgments

The work was partly supported by DFG grant RE 322/11-1 as well as the grants Heisenberg - Landau (Germany - BLTP JINR) and Votruba - Blokhintsev (Czech Republic - BLTP JINR) for 2007 and 2008 years. W.K. and P.-G.R. are grateful for the BMBF support under contracts 06 DD 139D and 06 ER 808. This work is also a part of the research plan MSM 0021620859 supported by the Ministry of Education of the Czech Republic. It was partly funded by Czech grant agency (grant No. 202/06/0363) and grant agency of Charles University in Prague (grant No. 222/2006/B-FYZ/MFF).

- 
- [1] B.L. Berman and S.C. Fultz, *Rev. Mod. Phys.* **47**, 713 (1975).
- [2] A. van der Woude, *Prog. Part. Nucl. Phys.* **18**, 217 (1987).
- [3] K. Langanke and M. Wiescher, *Rep. Prog. Phys.* **64**, 1657 (2001).
- [4] M. Goldhaber and E. Teller, *Phys. Rev.* **74**, 1046 (1948).
- [5] H. Steinwedel and J.H.D. Jensen, *Z. Naturforsch* **5a**, 413 (1950).
- [6] D. J. Rowe, *Nuclear Collective Motion* (Methuen, London, 1970).
- [7] G. E. Brown, *Unified Theory of Nuclear Models and Forces* (North-Holland, Amsterdam, 1971).
- [8] K. Goeke and J. Speth, *Ann. Rev. Nucl. Part. Sci.* **32**, 65 (1982).
- [9] J. Speth and J. Wambach, *Int. Rev. Nucl. Phys.* **7**, 1 (1991).
- [10] G. F. Bertsch and R. Broglia, *Oscillations in Finite Quantum Systems* (Cambridge University Press, Cambridge, 1994).
- [11] M. Bender, P.-H. Heenen, and P.-G. Reinhard, *Rev. Mod. Phys.* **75**, 121 (2003).
- [12] D. Vretenar, A.V. Afanasjev, G.A. Lalazissis, and P. Ring, *Phys. Rep.* **409**, 101 (2005).
- [13] J. R. Stone and P.-G. Reinhard, *Prog. Part. Nucl. Phys.* **58**, 587 (2007).
- [14] R. M. Dreizler and E. K. U. Gross, *Density Functional Theory* (Springer, Heidelberg, 1990).
- [15] I. Zh. Petkov and M. V. Stoitsov, *Nuclear Density Functional Theory*, (Clarendon Press, Oxford, 1991).
- [16] T.H.R. Skyrme, *Phil. Mag.* **1**, 1043 (1956).
- [17] D. Vauterin, D.M. Brink, *Phys. Rev.* **C5**, 626 (1972).
- [18] Y.M. Engel, D.M. Brink, K. Goeke, S.J. Krieger, and D. Vauterin, *Nucl. Phys.* **A249**, 215 (1975).
- [19] S. Shlomo and G. F. Bertsch, *Nucl. Phys.* **A243**, 507 (1975).
- [20] S. Krewald, V. Klemt, J. Speth, and A. Faessler, *Nucl. Phys.* **A281**, 166 (1977).
- [21] P.-G. Reinhard, *Ann. Phys. (Leipzig)* **1**, 632 (1992).
- [22] P.-G. Reinhard, *Nucl. Phys.* **A649**, 305c (1999).
- [23] J.A. Maruhn, P.-G. Reinhard, P.D. Stevenson, J.R. Stone, and M.R. Strayer, *Phys. Rev. C* **71**, 064328 (2005).
- [24] V.O. Nesterenko, J. Kvasil, and P.-G. Reinhard, *Phys. Rev. C* **66**, 044307 (2002).
- [25] V.O. Nesterenko, W. Kleinig, J. Kvasil, P. Vesely, P.-G. Reinhard, and D.S. Dolci, *Phys. Rev. C* **74**, 064306 (2006).
- [26] V.O. Nesterenko, W. Kleinig, J. Kvasil, P. Vesely, and P.-G. Reinhard, *Int. J. Mod. Phys. E* **16**, 624 (2007).
- [27] V.O. Nesterenko, W. Kleinig, J. Kvasil, P. Vesely, and P.-G. Reinhard, *Proceed. of 26th Intern. Workshop on Nucl. Theory, Rila, Bulgaria, 2007*, edited by S. Dimitrova, (INRNE BAS, Sofia, 2007), p. 273.
- [28] V.O. Nesterenko, W. Kleinig, J. Kvasil, P. Vesely, and P.-G. Reinhard, *Int. J. Mod. Phys. E* **17**, 89, (2008).
- [29] E. Chabanat, P. Bonche, P. Haensel, J. Meyer, and R. Schaeffer, *Nucl. Phys.* **A635**, 231 (1998).
- [30] A.V. Varlamov, V.V. Varlamov, D.S. Rudenko, and M.E. Stepanov, *Atlas of Giant Dipole Resonances*, INDC(NDS)-394, 1999; JANIS database.
- [31] G.M. Gurevich, L.E. Lazareva, V.M. Mazur, S.Yu. Merkulov, G.V. Solodukhov and V.A. Tyutin, *Nucl. Phys.* **A351**, 257 (1981).
- [32] V.V. Varlamov, M.E. Stepanov, V.V. Chesnokov, *Bull. Russian Academy of Sciences, Ser. Fiz.* **67**, 724 (2003).
- [33] B.I. Goryachev, Yu.V. Kuznetsov, V.N. Orlin, N.A. Pozhidaeva and V.G. Shevchenko, *Yad.Fiz.* **23**, 1145 (1976).
- [34] A.M. Goryachev and G.N. Zalesnyy, *Vopr. Teor. Yad. Fiz.* **5**, 42 (1976).
- [35] A.M. Goryachev and G.N. Zalesnyy, *Yad. Fiz.* **26**, 465 (1977).
- [36] B.L. Berman, D.D. Faul, R.A. Alvarez, P. Meyer, and D.L. Olson, *Phys. Rev. C* **19**, 1205 (1979).
- [37] G.M. Gurevich, L.E. Lazareva, V.M. Mazur, G.V. Dolodovnikov, and B.A. Tulupov, *Nucl. Phys.* **A273**, 326 (1976).
- [38] B.L. Berman, J.T. Caldwell, E.J. Dowdy, S.S. Dietrich, P. Meyer, and R.A. Alvarez, *Phys. Rev. C* **34**, 2201 (1986).
- [39] J.T. Caldwell, E.J. Dowdy, B.L. Berman, R.A. Alvarez, and P. Meyer, *Phys. Rev. C* **21**, 1215 (1980).
- [40] M. Bender, K. Rutz, P.-G. Reinhard, J. A. Maruhn, and W. Greiner, *Phys. Rev. C* **60** 034304 (1999).
- [41] M. Bender, W. Nazarewicz, and P.-G. Reinhard, *Phys.*

- Lett. B **515**, 42 (2001).
- [42] V.V. Varlamov and B.S. Ishkhanov, Phys. Part. Nucl. **35**, 859 (2004).
- [43] S. Raman, At. Data and Nucl. Data Tables **36**, 1 (1987).
- [44] M. Brack and W. Stocker, Nucl. Phys. **A406**, 413 (1983).
- [45] W.D. Myers, W.J. Swiatecki, T. Kodama, L.J. El-Jaick, and E.R. Hilf, Phys. Rev. C **15**, 2032 (1977).
- [46] A. Baran, Z. Lojewski, K. Sieja, and M. Kowal, Phys. Rev. C **72**, 044310 (2005).